Contents lists available at ScienceDirect

Optics and Laser Technology

journal homepage: http://ees.elsevier.com

Full length article

Effect of laser pulse duration on properties of metal and metal carbide nanoparticles obtained by laser in liquid synthesis

M. Curcio [a], A. De Bonis [a,*], A. Santagata [b], A. Galasso [a], R. Teghil [a]

[a] Dipartimento di Scienze, Università della Basilicata, Viale dell'Ateneo Lucano, 10, 85100 Potenza, Italy
[b] CNR-ISM-UOS Tito Scalo, C.da S. Loja, 85050 Tito Scalo, Pz, Italy

ARTICLE INFO

Keywords
Ultrashort laser ablation in liquid
Short laser ablation in liquid
Transition metal carbides
Nanoparticles growth mechanism

ABSTRACT

The control of the parameters that affect the physic-chemical properties of nanoparticles obtained by laser ablation in liquid is of relevant importance to select size and composition of materials suitable for applications such as catalysis and biomedical materials. We have focused our attention on the role of laser pulse lenght on the dimension, composition and crystallinity of laser synthesized particles. We observed that the ablation in water and organic solvents with short laser source allows to achieve particles with large crystalline domains, usually.Pd particles with a median diameter of 7 nm and 10 nm and crystalline domain of 28 nm and 45 nm were obtained by fs and ns ablation in water, respectively. Particles wrapped in carbon shells were observed by ns ablation of transition metals in organic liquid. The decomposed organic molecules absorbed on the growing particles can hinder their coalescence, therefore smaller particles were obtained by ns ablation with respect to particles obtained by fs ablation in the same experimental conditions. HR-TEM and XRD analysis allow to state that, MoC, TaC and WC_{1-x} particles were obtained both by fs and ns metals ablation in toluene and ns ablation in acetone. By ultrashort laser ablation of Mo, Ta and W in acetone MoC, Ta_4C_3 and WC_{1-x} + WO_x particles were observed, respectively.

1. Introduction

The growing interest in laser ablation in liquid (LAL) technique in the last years is due to the possibility to obtain nanoparticles (NPs) that retain the target stoichiometry or whose composition is mediated by the liquid environment without the use of toxic reagents and extreme temperature and pressure conditions [1]. The ablation of a solid target in liquid gets to the formation of a hot plasma, the vaporization of the surrounding liquid and the formation of a micrometric cavitation bubble (CB) where target atoms and clusters and liquid species can react at high pressure, high temperature conditions. The quickly cooling at room temperature of the ablation products takes place as soon as they are released in the surrounding liquid. Since it has been shown that all the ablated material takes part in NPs formation, LAL is a high efficient technique for the NPs production [2].

Dynamics of the ablation process depends on many experimental parameters, the most relevant are liquid and target physico-chemical properties and laser wavelength, pulse duration and repetition rate. The knowledge and control of all these parameters are necessary to predict the LAL products size and composition. It has been recognized that pulse duration is one of the key parameters that affects the ablation process, lifetime and dimension of the CB, yield and size distribution of the obtained nanoparticles [3]. In the CB the nucleation and growth of NPs take place, particles dimension and composition are scarcely modified in the room temperature solvent [4]. Shape and lifetime of laser induced CB depend on laser fluence and pulse duration, target geometry and surface morphology [5]. Irrespective from these evidences, it has been observed that the influence of volume and shape of the laser induced CB on the particle size is not relevant. Letzel et al. [6] studied the effect of the re-irradiation of a single ablation spot on the size dimension of NPs obtained by LAL. They show that by increasing the number of laser shots on the same spot, the size and lifetime of CB decrease, on the other hand the nanoparticles size distribution is not strongly affected. They suggested that the ablation mechanism is more important determining particles dimension.

It is widely recognized that different mechanisms could be at the origin of formation and growth of particles obtained by LAL [5,7,8]. In particular, smaller particles are formed by gas condensation inside the CB (primary). The origin of larger particles (secondary) is unclear and could be dependent on the laser pulse duration. The generation of secondary particles obtained during the ps laser ablation of gold and silver

* Corresponding author.
E-mail address: angela.debonis@unibas.it (A. De Bonis)

https://doi.org/10.1016/j.optlastec.2021.106916
Received 10 June 2020; Received in revised form 3 November 2020; Accepted 4 January 2021
Available online xxx
0030-3992/

in water has been investigated by spatially and time resolved X-ray techniques. The appearance of particles with crystal domains of about 20 nm in front of the emerging CB has been demonstrated and has been related to a liquid layer break up and jetting droplets effect [8]. On the other hand, the effect of pulse duration on the structure and composition of the LAL products has been scarcely investigated. De Bonis et al. compared the products of the ablation of GaAs target in acetone with nanosecond and femtosecond sources, observing that the ultrashort ablation allows to obtain NPs that retain the target stoichiometry, on the other hand, by nanosecond ablation particles with a Ga/As ratio of 1.4 were obtained. The authors explain the observed difference considering that different ablation mechanisms are effective with the two laser sources and justified the gallium excess with the melting effect usually observed during nanosecond laser ablation [9]. Giorgetti et al. [10] observed that anatase and rutile phases were obtained by laser ablation of a titanium target in water with ps and ns laser sources, respectively. They evaluate the yields of anatase and rutile considering the pressure and temperature evolution of the laser induced plume in the two temporal regimes and the phase diagram of TiO_2. Zhang et al., studied the ablation of an Al target in water with ns, ps, and fs laser sources and observed that morphology and composition of the obtained nanomaterials depend on the laser pulse length [11].

The mechanism of ns and fs laser ablation in vacuum has been widely studied and clarified [12,13] however, the knowledge of laser matter interaction in vacuum cannot be easily applied to LAL where the interaction with the liquid environment has a relevant role in the generation of NPs.

Theoretical [7,14,15] and experimental [8] investigations describe the ultrashort laser ablation in liquid considering that the impinging laser leads to the rapid heating and explosive decomposition of the target surface, with the ejection of vapour and hot liquid from the target. By theoretical models it has been evaluated that at the interface with the liquid the hot expanding plume is decelerated and the liquid reaches a supercritical state [7,14,15]. In these conditions, the nucleation of small nanoparticles takes place together with the formation of an expanding CB. After few nanoseconds, large liquid droplets, induced by hydrodynamic instability, are ejected in liquid environment, justifying the nanoparticles bimodal size distribution usually recognized in ultrashort LAL [14]. By ns LAL wider size distributions are usually observed, suggesting that alternative mechanisms could be effective for the formation of large NPs. Considering the ablation of metals in vacuum, during the interaction of the ns laser with the target surface, the absence of thermal and stress confinement on the target allows an ablation mechanism that Shin et al. [7] called “gentler” with respect to the ultrashort one. On the basis of these considerations, Shin et al. [7] proposed that the formation of nanomaterials during ns laser ablation in liquid take place without the ejection of droplets directly in the liquid, but all the formed nanoparticles cool down in the CB and are released in the surrounding environment during the bubble collapsing stage [7].

Laser ablation of metal target in water was proposed as a valid synthetic strategy for the preparation of metal NPs suitable for catalytic [16–18] or biomedical applications [19,20]. Moreover, great effort was spent for the synthesis of Transition Metal Carbides (TMC) NPs by LAL. TMC is a class of compounds that presents many interesting applications ranging from biomaterials [21] to mechanical reinforcement [22]. Their most interesting property is their catalytic activity. Promising W, Mo and Cr carbide nanomaterials have been proposed as low-cost electro-catalyst to decrease the over-potential of Li-O_2 or Li-S batteries [23,24]. TMC are obtained by multistep mechanism and the use of toxic reagents, usually. Recently, many authors reported the ablation of transition metals in alcohols, acetone, alkanes and aromatic solvents, by short and ultrashort laser pulses [25–31]. It has been observed that during the ablation of transition metals in organic solvents, the decomposition of the solvent provides carbon atoms and cluster that easily dissolve in metals with 3d vacancies with the formation of TMC NPs [25].

We present the synthesis of NPs obtained by laser ablation of some transition metals in water and organic solvents by short and ultrashort laser sources. With the aim to highlight the effect of laser pulse length on the composition and structure of materials obtained in LAL experiments, we used two laser sources with the same repetition rate (10 Hz), similar wavelength (527 nm and 532 nm), similar fluence (15 J/cm^2 and 14 J/cm^2) but different pulse length (250 fs and 6 ns). First, we consider the ablation of Pd in water and compare our results with the models proposed for fs and ns ablation in liquid [7,8]. Then we expand the study to reactive LAL considering the fs and ns ablation of transition metals (Mo, Ta and W) in organic solvents. In these experiments solvents photo and thermal decomposition allows the synthesis of TMC nanoparticles, usually wrapped in a carboneous matrix (see Table 1).

2. Experimental

Metal targets (Pd, Mo, Ta and W) were purchased by Goodfellow. The ablation experiments were carried out in bi-distilled water (MilliQ), in acetone and toluene (Aldrich) by using ns (frequency doubled Quanta System-Nd:YAG, 532 nm, 7 ns, 10 Hz, 15 mJ) and fs (frequency doubled Light Conversion-Nd:glass 527 nm, 250 fs, 10 Hz, 3 mJ) laser sources. Spot diameters of 2.1 * 10^{-4} cm^2 and 1 * 10^{-3} cm^2 and fluence of 14 J/cm^2 and 15 J/cm^2, were measured for fs and ns laser source, respectively. Targets were put at the bottom of a glass cell filled with 30 ml of liquid. Laser was focused just on the target surface by means of a 50 mm focal lens passing through a column of 2 cm of liquid and focusing position was adjusted by a micrometric translator in each experiment. The solution was kept on a magnetic stirrer to insure the irradiation uniformity (homogeneity) of the solvent and targets were continuously moved by means of a linear stage. All the ablations that last 30 min. Colloidal NPs collected onto Si (1 0 0) wafer were used for XRD and XPS analysis. XRD measurements were carried out by means of a XPerthD-5000 diffractometer equipped with Cu Kα radiation source. The average crystallite size were calculated using the well-known Scherrer equation:

$$D = \frac{k\lambda}{\beta cos\vartheta}$$

where k is a shape factor, λ is the Cu Kα radiation wavelength, β is the FWHM and θ is the Bragg angle of the selected peak. The instrumental broadening of the FWMH of the diffraction peaks was measures by using a standard provided by the instrument manufacturer and the following equation was used for correction [32]

Table 1
Median diameter, crystalline phase and crystallite size of nanopaticles obtained by laser ablation in liquid.

	Crystallite size	Crystalline phase	Median NPs size
Pd_water_fs	28 nm	Pd	7 nm
Pd_water_ns	45 nm	Pd	10 nm
Mo_acetone_fs	12 nm	MoC	12 nm
Mo_acetone_ns	27 nm	MoC	5 nm
Mo_toluene_fs	10 nm	MoC	9 nm
Mo_toluene_ns	26 nm	MoC	7 nm
Ta_acetone_fs	14 nm	Ta_4C_3	19 nm
Ta_acetone_ns	36 nm	TaC	9 nm
Ta_toluene_fs	21 nm	TaC	19 nm
Ta_toluene_ns	40 nm	TaC	5 nm
W_acetone_fs	15 nm	WC_{1-x} + WO_x	9 nm
W_acetone_ns	34 nm	WC_{1-x}	11 nm
W_toluene_fs	16 nm	WC_{1-x}	
W_toluene_ns	36 nm	WC_{1-x}	

$$\beta = (\beta_m - \beta_i)\sqrt{(\beta_m^2 - \beta_i^2)}$$

where β is the residual broadening of the peak, β_m is the FWHM of XRD diffraction peak, and β_i is the instrumental broadening.

XPS measurements were performed by using LH-Leybold X1 instrument. The acquired XPS spectra were analyzed by a curve-fitting program, Googly that allows the simultaneous fitting of peaks in the form of a Voigt function and their associated background in a wide energy range [33].

Nanoparticles median size was determinated by TEM analysis, by using a Fei-TECNAI G2 20 TWIN instrument. Few drops of the colloidal solutions obtained in LAL experiments were dropped onto holey carbon films copper grids.

UV spectra were registered for colloidal solutions obtained by laser ablation in water using a Specord 50 Plus – Analytik Jena spectrophotometer.

3. Results

3.1. fs and ns ablation of Pd in water

The ablation of Pd in water allows to obtain metallic nanoparticles with an amorphous oxide shell [16]. Size distribution of NPs obtained by fs source presents the typical bimodal profile, centred at 6 nm and 22 nm respectively (Fig. 1a, b) and with a median diameter of 7 nm. High resolution image (Fig. 1e) allows to recognize lattice distances of 0.22 nm, that can be referred to (1 1 1) planes of FCC crystal structure of metallic Pd. Crystallites of 28 nm have been evaluated by the Scherrer formula considering the peak at 40.0° of metallic Pd (01–088-2335) in the XRD spectrum reported in Fig. 2a. Nanosecond ablation gets to the formation of spherical higly interconnected NPs characterized by a monomodal size distribution (Fig. 1c and d) centred at 10 nm. Crystal lattice distance of 0,22 nm has been observed (Fig. 1f) and the XRD spectrum is very similar to that of fs produced Pd NPs, but larger crys-

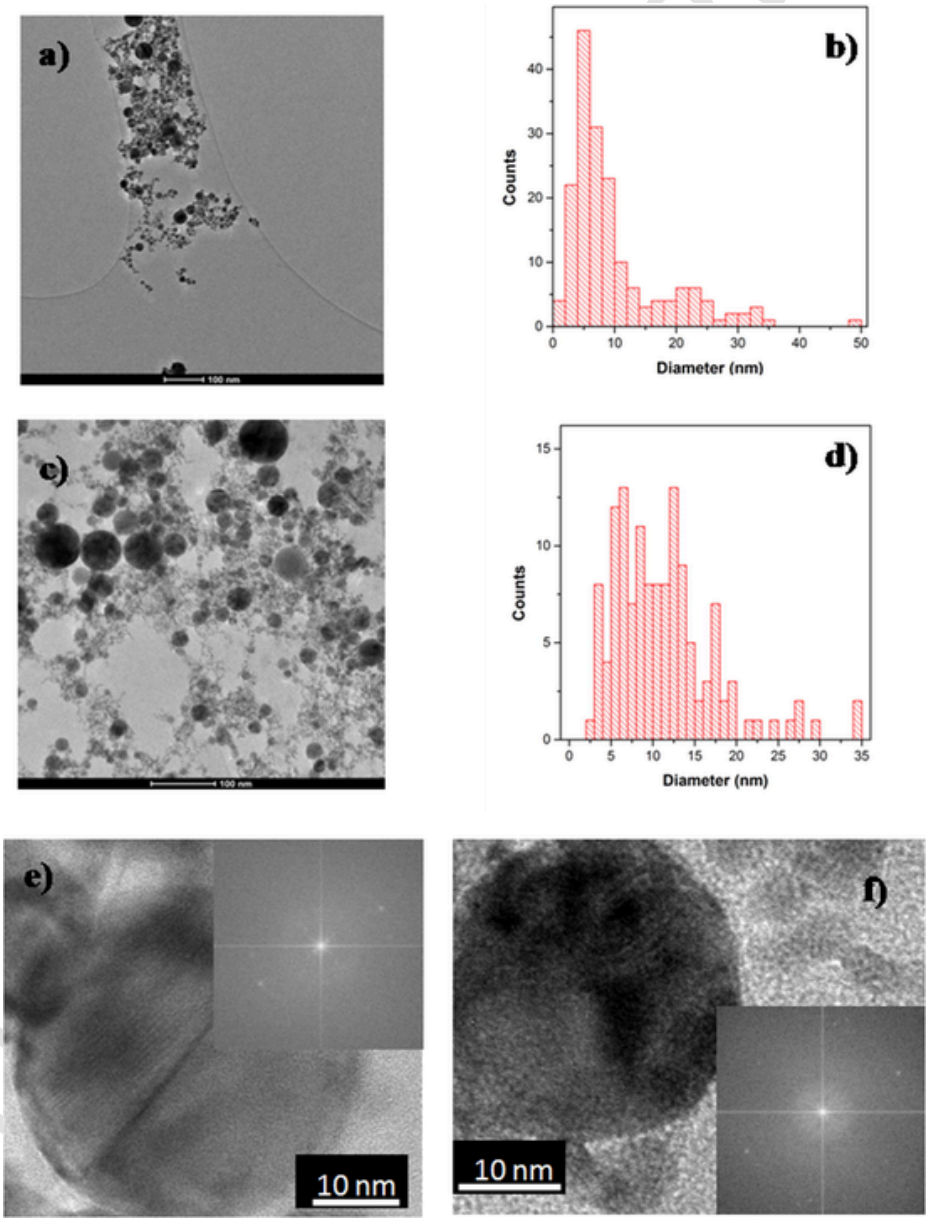

Fig. 1. TEM image (a), size distribution (b) and 2D FFT of the enlarged area (e) of NPs obtained by fs laser ablation of Pd in water; TEM image (c), size distribution (d) and 2D FFT of the enlarged area (f) of NPs obtained by ns laser ablation of Pd in water.

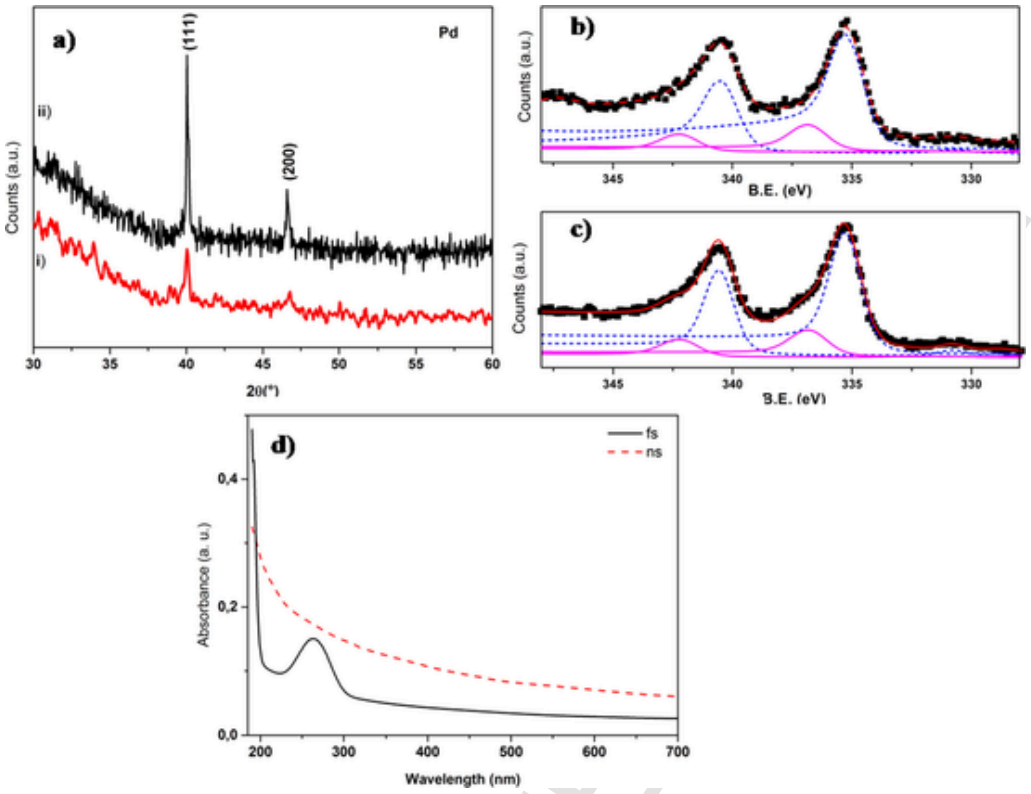

Fig. 2. (a) XRD pattern of Pd NPs synthesized with fs (i) and ns (ii). (b) Pd 3d region of NPs obtained by fs laser ablation of Pd in water, (c) Pd 3d region of NPs obtained by ns laser ablation of Pd in water; blue dotted lines refer to Pd $3d_{5/2}$ and Pd $3d_{3/2}$ of metallic Pd and magenta solid lines refer to Pd $3d_{5/2}$ and Pd $3d_{3/2}$ of palladium oxide. (d) UV–Vis spectra of colloidal solution obtained by ablation of Pd in water with fs (black solid line) and ns (red dashed line) laser sources.

tallites (45 nm) have been obtained by ns ablation. In Fig. 2b and c are reported Pd3d peaks of particles obtained by fs and ns Pd ablation in water, respectivley. $Pd3d_{5/2}$ signals are composed by a doublet centred at binding energy (B.E.) 336.7 and 335.1 eV and assigned to PdO and metallic Pd species, respectively [34]. The amount of palladium oxide (about 20%) on the surface of the NPs obtained by fs and ns ablation is very similar, irrespective from the laser pulse length used in the experiments.

UV–Vis spectra of the colloidal solution obtained by fs and ns ablation of Pd in water are reported in Fig. 2 d. UV spectrum of ns obtained Pd particles is typical for nanometer sized metallic species, it doesn't present a well definite surface plasmon band but a very large band extending into the UV that can be related to an intraband transition of a metallic system [35]. Absorption spectrum of colloidal solution obtained by fs ablation of Pd in water is very different: a high peak below 200 nm and a smaller peak at about 265 nm, that can be associated to oxidized Pd species, are visible and the absorbance all over the spectrum is lower than that of the spectrum acquired for ns obtained colloids.

3.2. Transition metals in organic solvents: Formation of transition metal carbides

With the aim to highlight the effect of laser pulse duration on the formation of metal carbide NPs during LAL in organic solvents, we have studied the ablation of Mo, Ta and W in acetone and toluene by short and ultrashort laser sources.

Short and ultrashort laser ablation of Mo in acetone and toluene get to the formation of MoC nanoparticles, as suggested by the observed lattice distance of 0.24 nm that can be assigned to cubic MoC (1 1 1) (Fig. 3i) [26]. By TEM images it was possible to evaluate that particles obtained by ultrashort source are larger with respect to particles obtained by ns laser (median size of 9 and 7 nm in toluene and 12 and 5 nm in acetone, respectively) (Fig. 3a–h). A lighter amorphous matrix envelops NPs obtained by ns ablation in acetone; in this case, the amorphous network is much more evident for ablation carried out in toluene. The graphitization of the amorphous carbon on the NPs surface gets to the formation of Onion Like Carbon (OLC) shells that wrap particles obtained by ns laser ablation in acetone (Fig. 3j) and more extensively by both laser sources ablation in toluene. XRD spectra reported in Fig. 4a and b present the signals of MoC phase (03-065-0280) with crystalline domains of 12 and 27 nm for NPs obtained in acetone and 10 and 26 nm for NPs obtained in toluene, for fs and ns ablation, respectively (Fig. 4a and b). XPS analysis of NPs obtained by fs and ns ablation of Mo in acetone and toluene are reported in Fig. 4c and d. In all spectra, Mo 3d doublets are composed by two components. The $Mo3d_{5/2}$ components centred at 232.7 and 228.3 eV can be related to Mo^{+6} and molybdenum carbide species, respectively. Particles obtained by Mo ablation in toluene are composed by a higher amount of molybdenum carbide with respect to material obtained by ablation in acetone (about 55% and 35%, respectively), irrespectively from the laser pulse length. The low intensity of Mo3d signal for particles obtained by ns laser ablation in toluene suggests can be related to the higher amount of decomposed solvent that envelops NPs, as TEM images (Fig. 3c and g) suggest.

By fs laser ablation of Ta in acetone spherical core/shell NPs with a median diameter of 19 nm have been obtained (Fig. 5a and b). The lighter shell does not show any evidence of OLC structure (Fig. 5i). Polycrystalline particles with lattice distances of 0.25 nm are present. This lattice distance can be related to Ta_4C_3(1 1 1) crystal planes [26]. XRD analysis (Fig. 6a) confirms the presence of Ta_4C_3 phase (01-089-2121) and crystal domains of 14 nm were evaluated by Scherrer method. NPs obtained by short LAL in acetone have median size of 9 nm (Fig. 5c and d). Lattice distance of 0.26 nm that can be assigned

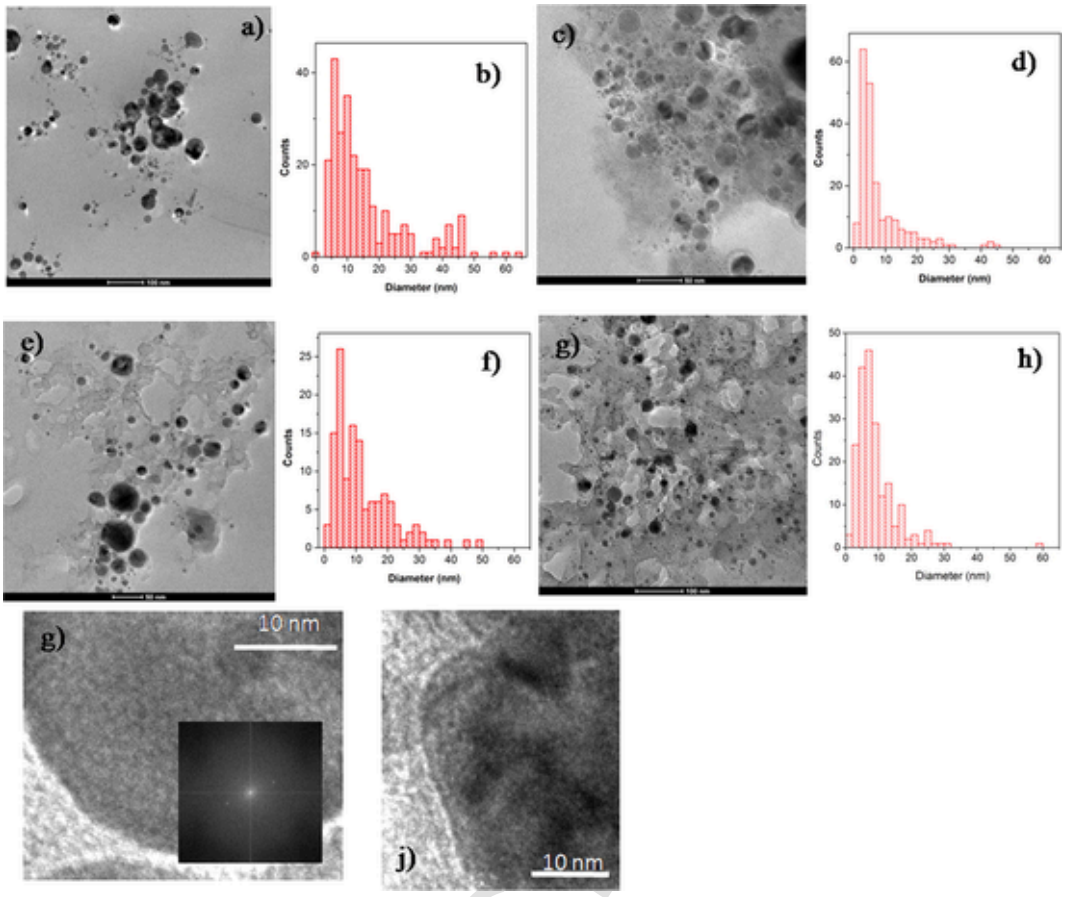

Fig. 3. TEM image and size distribution of NPs obtained by fs (a, b) and ns (c, d) laser ablation of Mo in acetone; TEM image and size distribution of NPs obtained with fs (e, f) and ns (g, h) laser ablation of Mo in toluene; enlarged area and 2D –FFT of NPs obtained by fs ablation of Mo in acetone (i); enlarged area of NPs obtained by ns ablation of Mo in acetone (j).

to (1 1 1) planes of cubic TaC phase were observed. XRD analysis (Fig. 6a) allows to state that TaC(03-065-0282) NPs have crystal domains of 36 nm. By using toluene as liquid environment, OLC/TaC core/shell NPs were obtained both by ultrashort and short laser sources (Fig. 5h). In both experiments crystalline particles with lattice distance of 0.26 nm were observed. By short laser ablation many particles with a diameter <10 nm are embedded in a lighter amorphous matrix, probably due to the toluene decomposition. NPs size distributions centred at 19 and 5 nm (Fig. 5f and h) and crystal domains of 21 nm and 40 nm (Fig. 6b) were evaluated for particles obtained by ultrashort and short LAL in toluene, respectively.

W ablation in acetone by using ultrashort and short laser source gets to the formation of NPs with similar median size (9 and 11 nm, respectively) (Fig. 7a–d). The lattice distance observed of 0.24 nm can be related to cubic WC_{1-x} (1 1 1) planes (Fig. 7e) [25]. Contrary to what observed for Ta and Mo, few layers OLC structures wrapping NPs obtained by fs laser ablation of W in acetone have been observed (Fig. 7f). XRD spectra of particles obtained by W ablation in acetone and in toluene (Fig. 8a and b) show that WC_{1-x} carbide phase (00-020-1316) was obtained and confirm that larger crystalline domains were formed during ns ablation with respect to fs (16 and 36 nm in toluene and 15 and 34 nm in acetone, respectively). It should be noted that in XRD spectrum of particles obtained by fs ablation in acetone a broad band centred at 33.2° is present. This peak can suggest the presence of tungsten trioxide (WO_3 – 01-087-2403).

4. Discussion

The effect of laser pulse duration on the size distribution of NPs obtained by ablation of metal targets in liquid has been already reported and discussed [7,36,37]. Usually, NPs obtained by fs laser sources are smaller with respect to NPs obtained by ns laser sources in the same experimental conditions [36,37]. fs ablation gets NPs with bimodal size distributions and Kabashin et al. suggested that larger NPs could be related to a melting effect due to the CB collapse [36]. Recently, it has been proposed that NPs formation by LAL starts in the laser induced plasma thanks to the non equilibrium conditions allowed by the interaction between the hot plasma and the surrounding liquid and the plasma high cooling rate that has been evaluated of 10^{12} Ks^{-1} for fs-LAL and more than 10^{10} Ks^{-1} for ns-LAL [5]. Reich et al. [8] studied the formation and growth of metal nanoparticles during laser ablation in liquid with ps laser sources using SAXS and WAXS time resolved pump–probe techniques. They showed that by ultrashort laser ablation in liquid two different mechanism of particles generation are effective. Smaller particles (primary particles) grow inside the CB in the first 50–300 ns after the ps laser pulse. Taccogna et al. highlighted the role of the laser induced plasma in NPs formation and proposed that the competition between electrostatic growth and atom evaporation could be at the origin of the primary particles formation [2]. These particles, homogenously dispersed inside the CB, have crystalline domains of about 8 nm. At the same time, particles with crystalline domains of 15–20 nm accumulate in the upper part of the bubble and/or precede the bubble. Reich et al. [8] proposed that the formation of these larger particles can be related to a jetting effect from a propagating melted metal layer and can be at the origin of the bimodal size distribution usually reported for laser ablation with ps-fs laser sources [35,36]. These results are supported by the atomistic simulations that describe the laser ablation in the ps regime highlighting the critical role of the hot molten metal layer in contact with the liquid environment in the NPs genera-

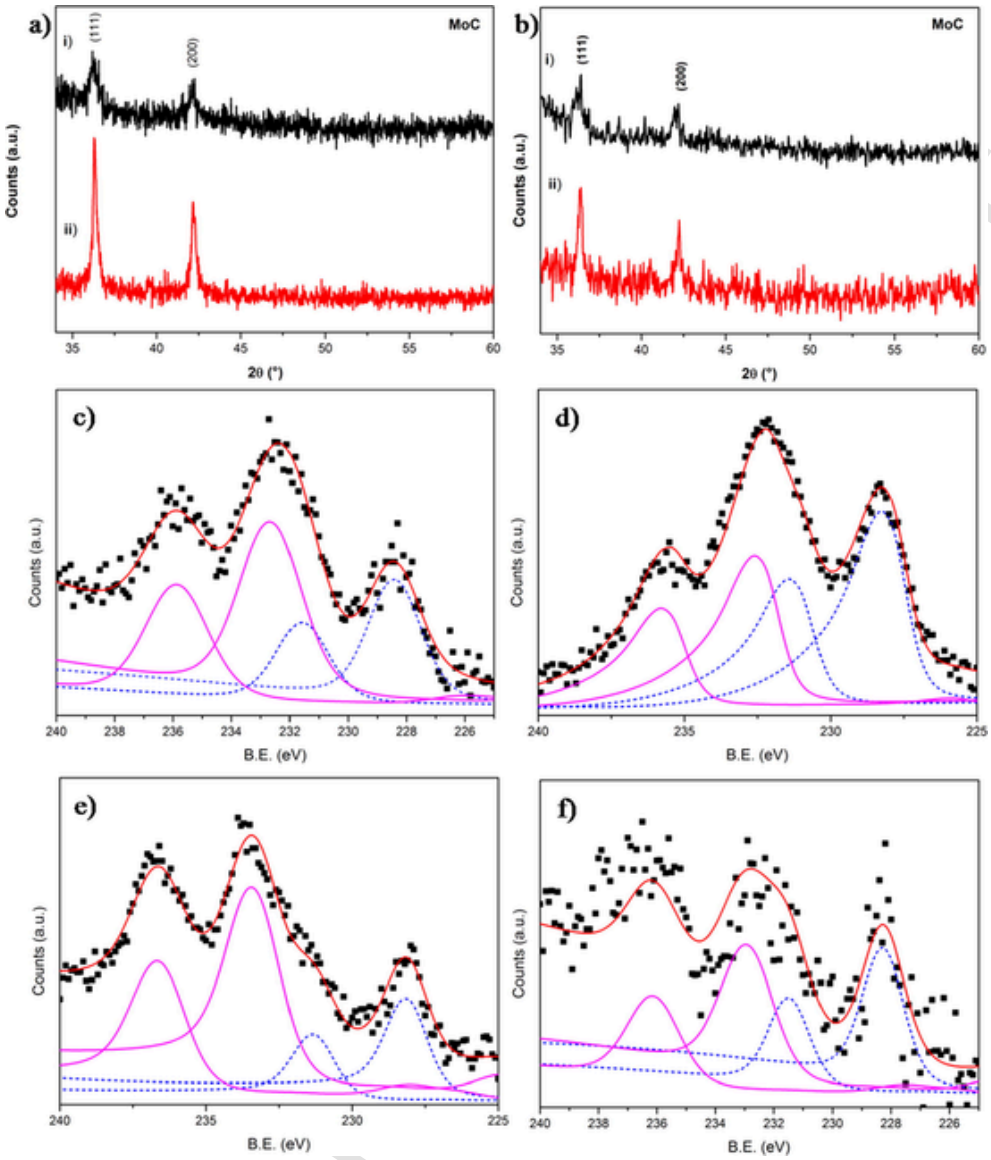

Fig. 4. XRD pattern of molybdenum carbide NPs synthesized with fs (i) and ns (ii) ablation in acetone (a) and in toluene (b); XPS spectra of Mo3d region of NPs synthesized with fs (c) and ns (e) ablation in acetone and fs (d) and ns (f) ablation in toluene.

tion mechanism. In this model the hot liquid layer serves as reserve of metal atoms for the nucleation of particles in the laser induced cavitation bubble and, at the same time, due to hydrodynamic instability, readily disintegrates with the formation of nanojets that release 10–20 nm droplets into the liquid environment. These droplets, in contact with the cold environment, rapidly cool down and solidify [7,14]. Atomistic simulation that describes the ablation in liquid mechanism considering longer laser pulses (τ > 400 ps) has been recently proposed [7]. The main differences between short and ultrashort laser ablation are the characteristic times of redistribution of the laser energy in the target by thermal conduction and stress waves. Considering the ablation of Ag in water, Shih et al. [7] estimated that by using 400 ps or longer laser pulses, thermal diffusion and mechanical relaxation in the metal target are allowed, getting to an ablation mechanism, that they defined "gentler", without the ejection of metal droplets in the liquid environment, as proposed for laser ablation performed with shorter laser pulses. By using short laser pulses (τ > 400 ps) three mechanisms for nanoparticles generation have been suggested: (i) the decomposition of a thin metal layer at the interface between the ablation plume and the liquid, (ii) the vapour mediated nucleation of small particle and (iii) the spinodal decomposition of a part of the ablation plume with the formation of large particles. Moreover, the high temperature in the CB allows the collision and coalescence of small particles and the growth of larger ones. In this context, the formation of particles with larger crystalline domains by ns laser ablation can be understood. ns induced NPs nucleate in a laser induced plasma that cools down slowly with respect to the fs one and grow inside the CB. Moreover, it is widely known that ns induced CB has longer lifetimes with respect to CB induced by fs ablation [9]. So, NPs formed by ns ablation rest hundreds of microseconds in the CB gaseous environment getting to a slower cooling down and higher growth of crystal domains with respect to jetted fs induced NPs.

The experimental results obtained by laser ablation of Pd in water by fs and ns laser sources are in good agreement with the model proposed by Shih et al. [7]: particles obtained by fs ablation have a bimodal size distribution and smaller crystalline domains with respect to that obtained by ns ablation in the same experimental conditions.

The scenario could be different considering the ablation of reactive transition metals in organic solvents where the hot plasma in contact with the liquid might result a suitable environment for metal reactivity.

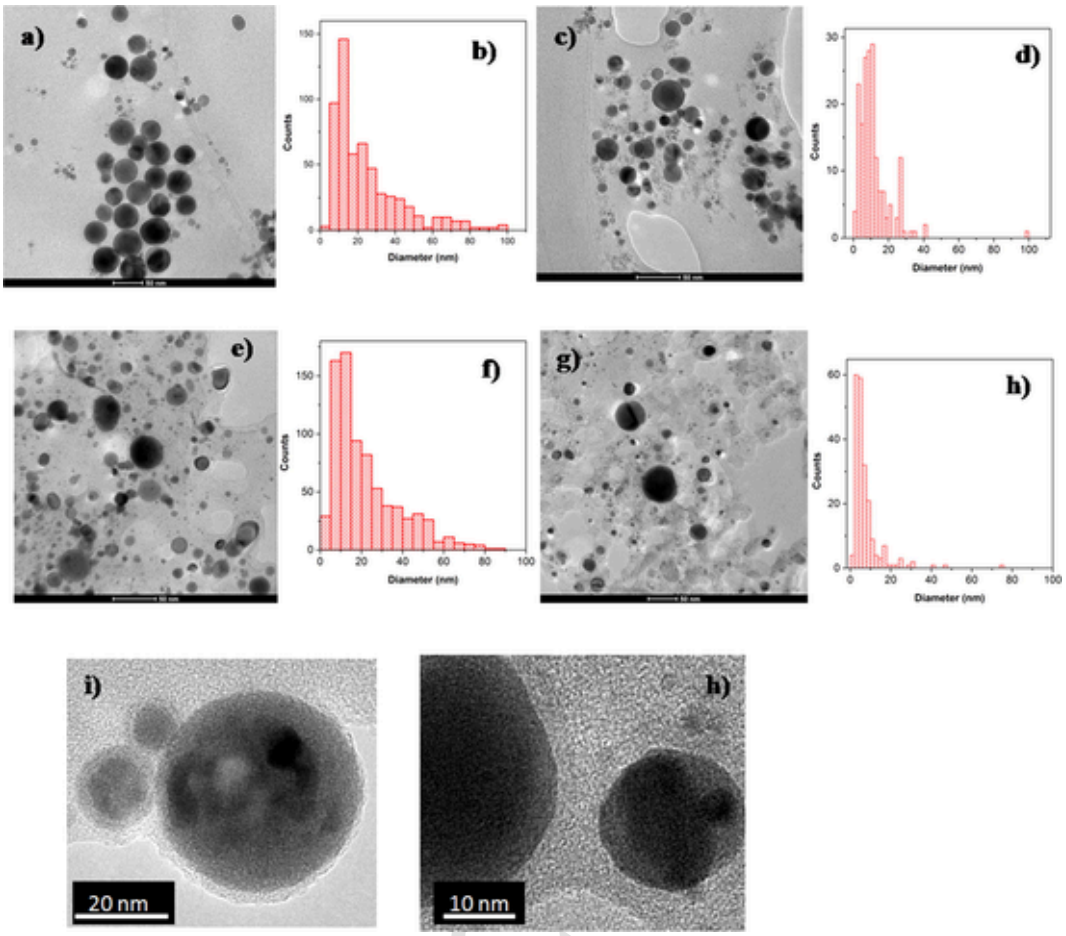

Fig. 5. TEM image and size distribution of NPs obtained by fs (a, b) and ns (c, d) laser ablation of Ta in acetone; TEM image and size distribution of NPs obtained with fs (e, f) and ns (g, h) laser ablation of Ta in toluene; enlarged area of NPs obtained by fs ablation of Ta in acetone (i); enlarged area of NPs obtained by fs ablation of Ta in toluene (j).

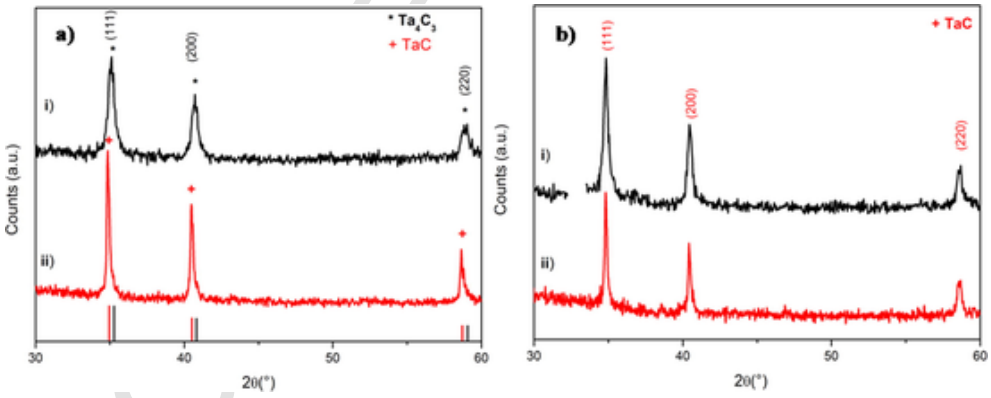

Fig. 6. XRD pattern of tantalum carbide NPs synthesized in acetone (a) and in toluene (b) with fs (i) and ns (ii) laser ablation.

The interaction of an intense laser pulse with organic molecules can induce their vaporization and decomposition. The dissociation of organic molecules by ultrashort laser pulse [38] has been reported, but it has been proved that the presence of catalytic metallic nanoparticles (usually transition metals) is necessary to obtain the decomposition of molecules by ns laser sources [39]. In fact, during catalytic decomposition, d orbitals of the metallic target can transfer electronic charge to the adsorbate molecules allowing their dissociation. It has been proved also that the metal assisted decomposition rate changes varying the metal catalyst [39]. During laser ablation experiments in organic solvents, in the laser induced plasma are present a large amount of carbon atoms and clusters, hydrogen or oxygen radicals and carbon based fragments, depending on the solvent molecular composition. These species can quickly react with the ablated metal atoms, clusters and NPs [41] and the formation of metal carbides and/or metal oxide can start. At high temperature, carbon atoms easily dissolve into metal NPs, bounding to metal vacancies and forming metal carbides. In this condition metal electron configuration, number of d vacancies, affinity with respect to carbon and oxygen and thermodynamic properties together with the solvent composition determine the NPs properties [25]. Considering the ablation in acetone, its decomposition follows complex mechanisms that allow the formation of oxygen and hydrogen gases and radicals,

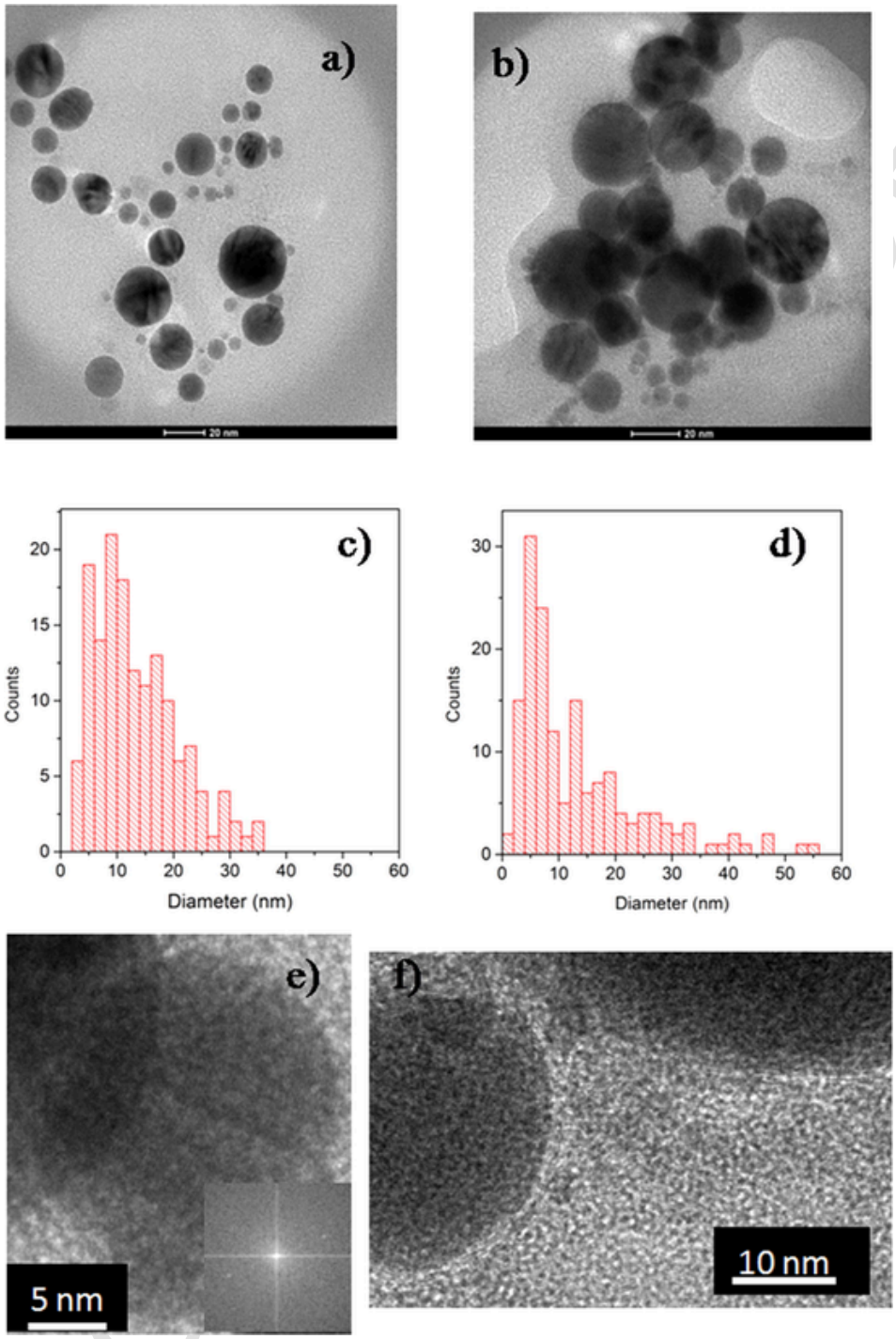

Fig. 7. TEM image and size distribution of NPs obtained with fs (a, c) and ns (b, d) laser ablation of W in acetone; enlarged area and 2D-FFT of NPs obtained by fs ablation of W in acetone (e, f).

radical ions and organic fragments [40], polyynes [41] and reductive gases such as CO, C_2H_6 and CH_4 [42]. In the bubble phase, where temperatures of some hundreds degrees have been predicted [43], metal carbonization can continue thanks to reactions such as [25]

$$2\,M(s) + xC_2H_6(g) \rightarrow 2MC_x(s) + 3xH_2(g) \quad (1)$$

In this context, we can consider that the metal carbonization in the bubble phase could have a relevant role to understand the differences observed during fs and ns ablation of Ta in acetone. Formation and growth of ns induced NPs take place in the CB, without ejection of NPs in the liquid environment before CB collapse, as predicted for fs ablation. In ns induced bubble higher equilibrium temperature [44] can be reached than in fs induced one and ns CB size and lifetime is about twice with respect to fs one [9], allowing a deeper carbonization of metal NPs and the formation of stoichiometric TaC thanks to (1). XPS analysis highlight that oxidized species are present on the surface of particles obtained by ns and fs ablation of Mo both in acetone and toluene. However, no crystalline oxide species have been observed by ns ablation of Ta, Mo and W in acetone, although oxygen is present in solvent molecular formula and the formation of reactive oxygen ions

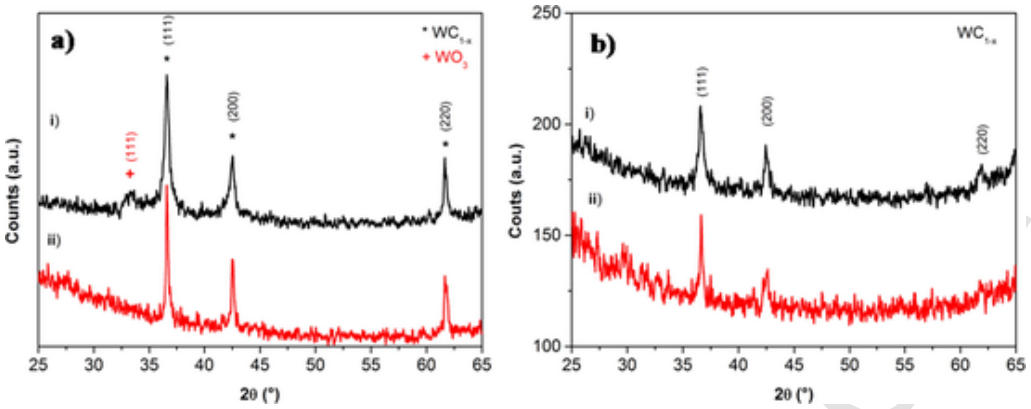

Fig. 8. XRD pattern of tungsten carbide NPs synthesized with fs (i) and ns (ii) ablation in acetone (a) and in toluene (b).

and radicals can be predicted. The presence of reductive gases that can get to a purification effect with the transformation of metal oxides into metals or metal carbide as suggested by Zhang et al. [25], can be invoked. The formation of crystalline metal oxides species by ns ablation in acetone of 4b-6b metals with high number of d vacancies is reported only for Zr that has higher affinity to oxygen atoms than to carbon atoms [25]. We suppose that the amorphous oxide species, observed in XPS spectra, were grown outside of the CB, probably due to the residual dissolved atmospheric gasses in the liquid environment, but their formation during the preparation of dry samples for XPS measurements cannot be definitively rule out. The presence of crystalline tungsten oxide during the fs ablation of W in acetone (Fig. 8a), confirms that different mechanisms of particles formation and growth are effective during short and ultrashort metal ablation in liquid.

Laser ablation of metals in toluene is a valid synthetic route for the easy preparation of core/shell materials where the shell has the OLC structure. The formation of OLC materials during laser ablation of metals in toluene is related to the aromatic solvent photodecomposition and high temperature pyrolysis. Toluene photolysis with ns laser source at fluence below the ablation threshold has been proposed at the origin of the formation of carbon onions structure grown onto silicon surfaces [44]. Toluene irradiation both by ns and fs laser sources gets to the formation of polyyne molecules with long carbon chain ($C_{20}H_2$) [45,46] and carbon–carbon triple bond moieties can be converted to carbon network in a carbonization process at high temperature [47]. Inside the CB, the high temperature pyrolysis of toluene can get to the formation of radicals, isomers and graphitic materials [48,49] that can adsorb onto the surface of the growing nanoparticles. The higher C amount that can be expected in the CB when the ablation is carried out in toluene with respect to acetone allows the formation of TaC stoichiometric phase both by short and ultrashort laser ablation.

Although it was confirmed that ns ablation allows to get particles with large crystalline domains, when organic solvents are used as liquid, smaller particles were obtained with respect to particles obtained by fs ablation. We can explain these results considering that by ns ablation the formation and growth of particles take place inside the CB [7], where a large amount of decomposed solvent molecules is present. These molecules can adsorb onto the particles surface and hinder their growth and coalescence. Particles are wrapped in a carbon shell that upon heating can evolve from amorphous to graphitic, thanks to the catalytic ability of the considered transition metals [50]. OLC shells were formed during fs and ns ablation in toluene and ns ablation of in acetone. Considering fs ablation in acetone, amorphous shells wrap Ta_4C_3 and MoC particles, while few OLC layers have been observed for tungsten carbide. We suggest that this different behaviour can be related to the very different thermal conductivity of tungsten carbide (110 W/mK) with respect to tantalum and molybdenum carbides (about 20 W/mK). The faster thermal exchange between the liquid environment and tungsten carbide, due to its higher thermal conductivity with respect to other metal carbides, can be at the origin of the formation of the OLC structures observed during fs laser ablation of W in acetone.

5. Conclusions

Among the many factors that affect laser synthesis of colloidal solution, we have focused our attention on the laser pulse length observing how this parameter plays a crucial role determining both particles dimension and crystalline size domains. It has been observed that by ns ablation particles with crystalline domains about twice with respect to fs ablation can be evaluated by Scherrer method. The ablation mechanism, nanoparticles generation and growth and CB dynamics can be invoked to understand this effect. ns ablation of Pd in water allows to obtain larger metallic Pd particles with respect to fs ablation. On the other hand, by using a reactive solvent such as acetone or toluene, the solvent decomposition pathways have to be considered to explain particles size and composition. By ns ablation, particles are formed and grow in the gaseous environment of the CB, allowing their extensive interaction with the vaporized and/or decomposed solvent molecules. We suppose that this effect can explain the observed formation of TaC and Ta_4C_3 phase by Ta ablation in acetone with ns and fs laser source, respectively. Particles obtained by ns ablation in acetone and toluene are usually smaller and wrapped in a carbonaceous environment that can hinder their coalescence and growth with respect to particles obtained by fs ablation in the same experimental conditions. Adsorbed molecules can limit carbidic particles oxidation, whereas hot particles ejected in the liquid before CB collapse during fs ablation can get to the formation of oxide phase as observed for tungsten.

Uncited reference

[51].

CRediT authorship contribution statement

M. Curcio: Methodology, Investigation, Data curation, Writing - original draft, Writing - review & editing. **A. De Bonis:** Conceptualization, Validation, Investigation, Data curation, Writing - original draft, Writing - review & editing, Supervision. **A. Santagata:** Methodology, Investigation. **A. Galasso:** Methodology, Investigation. **R. Teghil:** Conceptualization, Validation, Writing - original draft, Supervision.

Declaration of Competing Interest

The authors declare that they have no known competing financial interests or personal relationships that could have appeared to influence the work reported in this paper.

References

[1] V. Amendola, D. Amans, Y. Ishikawa, N. Koshizaki, S. Scirè, G. Compagnini, S. Reichenberger, S. Barcikowski, Room-temperature laser synthesis in liquid of oxide, metal-oxidecore-shells and doped oxide nanoparticles, Chem. – Eur. J. 26 (2020) 9206–9242.

[2] F. Taccogna, M. Dell'Aglio, M. Rutigliano, G. Valenza, A. De Giacomo, On the growth mechanism of nanoparticles in plasma during pulsed laser ablation in liquids, Plasma Sources Sci. Technol. 26 (2017) 045002 (10pp).

[3] K. Zhang, R.A. Ganeev, G.S. Boltaev, P.V. Redkin, C. Guo, Effect of different hardness and melting point of the metallic surface on structural and optical properties of synthesized nanoparticles, Mater. Res. Express 6 (2019) 045027.

[4] G. Marzun, H. Bonnemann, C. Lehmann, B. Spliethoff, C. Weidenthaler, S. Barcikowski, Role of dissolved and molecular oxygen on Cu and PtCu alloy particle structure during laser ablation synthesis in liquids, ChemPhysChem 18 (2017) 1175–1184.

[5] A. Kanitz, M.R. Kalus, E.L. Gurevich, A. Ostendorf, S. Barcikowski, D. Amans, Review on experimental and theoretical investigations of the early stage, femtoseconds to microseconds processes during laser ablation in liquid-phase for the synthesis of colloidal nanoparticles, Plasma Sources Sci. Technol. 28 (2019) 103001 (34pp).

[6] A. Letzel, M. Santoro, J. Frohleiks, A.R. Ziefus, S. Reich, A. Plech, E. Fazio, F. Neri, S. Barcikowski, B. Gokce, How the reirradiation of a single ablation spot affects cavitation bubble dynamics and nanoparticles properties in laser ablation in liquids, Appl. Surf. Sci. 473 (2019) 828–837.

[7] C.Y. Shih, M.V. Shugaev, C. Wu, L. Zhigilei, The effect of pulse duration on nanoparticle generation in pulsed laser ablation in liquids: Insights from large-scale atomistic simulations, Phys. Chem. Chem. Phys. 13 (2020) 7077–7099.

[8] S. Reich, A. Letzel, A. Menzel, N. Kretzschmar, B. Gokce, S. Barcikowski, A. Plech, Early appearance of crystalline nanoparticles in pulsed laser ablation in liquid dynamics, Nanoscale 11 (2019) 6962–6969.

[9] A. De Bonis, A. Galasso, A. Santagata, R. Teghil, Laser ablation of GaAs in liquid: the role of laser pulse duration, J. Phys. D: Appl. Phys. 49 (2016) 035301 (7pp).

[10] E. Giorgetti, M. Muniz-Miranda, S. Caporali, P. Canton, P. Marsili, C. Vergari, F. Giammanco, TiO2 nanoparticles obtained by laser ablation in water: Influence of pulse energy and duration on the crystalline phase, J. Alloys Compd. 643 (2015) S75–S79.

[11] K. Zhang, D.S. Ivanov, R.A. Ganeev, G.S. Boltaev, P.S. Krishnendu, S.C. Singh, M.E. Garcia, I.N. Zavestovskaya, C. Guo, Pulse duration and wavelength effects of laser ablation on the oxidation, hydrolysis and aging of aluminum nanoparticles in water, Nanomaterials 9 (2019) 767 (19pp).

[12] A. De Bonis, R. Teghil, Ultra-short pulsed laser deposition of oxides, borides and carbides of transition elements, Coatings 10 (2020) 501 (25pp).

[13] M.V. Shugaev, C. Wu, O. Armbruster, A. Naghilou, N. Brouwer, D.S. Ivanov, T.J.Y. Derrien, N.M. Bulgakova, W. Kautek, B. Rethfeld, L.V. Zhigilei, Fundamentals of ultrafast laser-material interaction, MRS Bull. 41 (2016) 960–968.

[14] C.Y. Shih, R. Streubel, J. Heberle, A. Letzel, M.V. Shugaev, C. Wu, M. Schmidt, B. Gökce, S. Barcikowski, L.V. Zhigilei, Two mechanisms of nanoparticle generation in picosecond laser ablation in liquids: the origin of the bimodal size distribution, Nanoscale 10 (2018) 6900–6910.

[15] Y.V. Petrov, V.A. Khokhlov, V.V. Zhakhovsky, N.A. Inogamov, Hydrodynamic phenomena induced by laser ablation of metal into liquid, Appl. Surf. Sci. 492 (2019) 285–297.

[16] A. Gentile, D. Giacco, A. De Bonis, R. Teghil, A.G. Marrani, S. Brutti, Synergistic electro-catalysis of Pd/PdO nanoparticles and Cr(III)-doped $NiCo_2O_4$ nanofibers in aprotic Li-O_2 batteries, J. Electrochem. Soc. 165 (2018) A3605–A3612.

[17] A. De Bonis, R. D'Orsi, M. Funicello, P. Lupattelli, A. Santagata, R. Teghil, L. Chiummiento, First application of homogeneous Pd nanoparticles prepared by pulsed laser ablation in liquid to a Suzuki-type reaction, Catal. Commun. 100 (2017) 164–168.

[18] S. Reichenberger, G. Marzun, M. Muhler, S. Barcikowski, Perspective of surfactant-free colloidal nanoparticles in heterogeneous catalysis, ChemCatChem 11 (2019) 4489–4518.

[19] A.L. Bailly, F. Correard, A. Popov, G. Tselikov, F. Chaspoul, R. Appay, A. Al-Kattan, A.V. Kabashin, D. Braguer, M.A. Esteve, In vivo evaluation of safety, biodistribution and pharmacokinetics of laser-synthesized gold nanoparticles, Sci. Rep. 9 (2019) 12890.

[20] V.A. Oleshchenko, A.Y. Kharin, A.F. Alykova, O.V. Karpukhina, N.V. Karpov, A.A. Popov, V.V. Bezotosnyi, S.M. Klimentov, I.N. Zavestovskaya, A.V. Kabashin, V.Y. Timoshenko, Localized infrared radiation-induced hyperthermia sensitized by laser-ablated silicon nanoparticles for phototherapy applications, Appl. Surf. Sci. 516 (2020) 145661 (7 pp).

[21] S.M. George, B. Kandasubramanian, Advancements in MXene-Polymer composites for various biomedical applications, Ceram. Int. 46 (2020) 8522–8535.

[22] N. Kang, W. Ma, L. Heraud, M. El Mansori, F. Li, M. Liu, H. Liao, Selective laser melting of tungsten carbide reinforced maraging steel composite, Addit. Manuf. 22 (2018) 104–110.

[23] F. Zhou, Z. Li, X. Luo, T. Wu, B. Jiang, L. Lu, H. Yao, M. Antonietti, S. Yu, Low cost metal carbide nanocrystals as binding and electrocatalytic sites for high performance Li–S batteries, Nano Lett. 18 (2018) 1035–1043.

[24] M. Christy, A. Arul, Y.B. Kim, Carbide composite nanowire as bifunctional electrocatalyst for lithium oxygen batteries, Electrochim. Acta 300 (2019) 186–192.

[25] D. Zhang, C. Zhang, J. Liu, Q. Chen, X. Zhu, C. Liang, Carbon-encapsulated metal/metal carbide/metal oxide core–shell nanostructures generated by laser ablation of metals in organic solvents, ACS Appl. Nano Mater. 2 (2019) 28–39.

[26] A. De Bonis, M. Curcio, A. Santagata, A. Galasso, R. Teghil, Transition metal carbide core/shell nanoparticles by ultra-short laser ablation in liquid, Nanomaterials 10 (2020) 145 (11pp).

[27] A. De Bonis, A. Santagata, A. Galasso, A. Laurita, R. Teghil, Formation of titanium carbide (TiC) and TiC core shell nanostructures by ultra-short laser ablation of titanium carbide and metallic titanium in liquid, J. Colloid Interface Sci. 489 (2017) 76–84.

[28] F. Davodi, E. Muhlhausen, D. Settipani, E. Rautama, A. Honkanen, S. Houtari, G. Marzun, P. Taskinen, T. Kallio, Comprehensive study to design advanced metal-carbide@graphene and metal-carbide@iron oxide nanoparticles with tunable structure by the laser ablation in liquid, J. Colloid Interface Sci. 556 (2019) 180–192.

[29] B.F. Mohazzab, B. Jaleh, O. Kakuee, A. Fattah-alhosseini, Formation of titanium carbide on the titanium surface using laser ablation in n-heptane and investigating its corrosion resistance, Appl. Surf. Sci. 478 (2019) 623–635.

[30] H. Zhang, J. Liu, Z. Tian, Y. Ye, Y. Cai, C. Liang, A general strategy towards transition metal carbide/carbon core/shell nanospheres and their application for supercapacitor electrode, Carbon 100 (2016) 590–599.

[31] H. Zhang, C. Liang, J. Liu, Z. Tin, G. Shao, The formation of onion-like carbon-encapsulated cobalt carbide core/shell nanoparticles by the laser ablation of metallic cobalt in acetone, Carbon 55 (2013) 108–115.

[32] C. Suryanarayana, M. Grant Norton, X-Ray Diffraction A Practical Approach, Springer, New York, 1998.

[33] J.E. Castle, A.M. Salvi, Chemical state information from the near-peak region of the X-ray photoelectron background, J. Electron Spectrosc. 114 (2001) 1103–1113.

[34] A. De Bonis, M. Sansone, A. Galasso, A. Santagata, R. Teghil, The role of the solvent in the ultrashort laser ablation of palladium target in liquid, Appl. Phys. A 117 (2014) 211–216.

[35] W. Chen, W. Cai, Y. Lei, L. Zhang, A sonochemical approach to the confined synthesis of palladium nanoparticles in mesoporous silica, Mater. Lett. 50 (2001) 53–56.

[36] A.V. Kabashin, Ph. Delaporte, A. Pereira, D. Grojo, R. Torres, Th. Sarnet, M. Sentis, Nanofabrication with pulsed lasers, Nanoscale Res. Lett. 5 (2010) 454–463.

[37] A. De Bonis, M. Sansone, L. D'Alessio, A. Galasso, A. Santagata, R. Teghil, Dynamics of laser-induced bubble and nanoparticles generation during ultra-short laser ablation of Pd in liquid, J. Phys. D Appl. Phys. 46 (2013) 445301.

[38] S. Wang, X. Tang, L. Gao, M.E. Elshakre, F. Kong, Dissociation of methane in intense laser field, J. Phys. Chem. A 107 (2003) 6123–6129.

[39] Z. Ghorbani, P. Parvin, A. Reyhani, S.Z. Mortzavi, A. Moosakhani, M. Maleki, S. Kiani, Methane decomposition using metal-assisted nanosecond laser-induced plasma at atmospheric pressure, J. Phys. Chem. C 118 (2014) 29822–29835.

[40] M.R. Kalus, N. Barsch, R. Streubel, E. Gokce, S. Barcikowski, B. Gokce, How persistent microbubbles shield nanoparticle productivity in laser synthesis of colloids – quantification of their volume, well dynamics, and gas composition, Phys. Chem. Chem. Phys. 19 (2017) 7112–7123.

[41] A. Hu, J. Sandeson, A.A. Zaidi, C. Wang, T. Zhang, Y. Zhou, W.W. Duley, Direct synthesis of polyyne molecules in acetone by dissociation using femtosecond laser irradiation, Carbon 46 (2008) 1823–1828.

[42] D. Yu, Z.Y. Tian, Z. Wang, Y.X. Liu, L. Zhou, Experimental and theoretical study on acetone pyrolysis in a jet-stirred reactor, Fuel 234 (2018) 1380–1387.

[43] M. Dell'Aglio, R. Gaudiuso, O. De Pascale, A. De Giacomo, Mechanism and processes of pulsed laser ablation in liquids during nanoparticles production, Appl. Surf. Sci. 348 (2015) 4–9.

[44] A. Vogel, J. Noack, K. Nahen, D. Theisen, S. Busch, U. Parlitz, D.X. Hammer, G.D. Noojin, B.A. Rockwell, R. Birngruber, Energy balance of optical breakdown in water at nanosecond to femtosecond time scales, Appl. Phys. B 68 (1999) 271–280.

[45] B.P. Dhong, D.E. Motaung, C.P. Liu, Y.C. Li, B.W. Mwakikunga, Nano-scale carbon onions produced by laser photolysis of toluene for detection of optical, humidity, acetone, methanol and ethanol detetction, Sens. Actuators, B 215 (2015) 30–38.

[46] Y. Taguchi, H. Endo, T. Kodama, Y. Achiba, H. Shiromaru, T. Wakabayashi, B. Wales, J.H. Sanderson, Polyyne formation by ns and fs laser induced breakdown in hydrocarbon gas flow, Carbon 115 (2017) 169–174.

[47] A. Ramadhan, M. Wesolowski, T. Wakabayashi, H. Shiromaru, T. Fujino, T. Kodama, W. Duley, J. Sanderson, Synthesis of hydrogen- and methyl-capped long-chain polyynes by intense ultrashort laser pulse irradiation of toluene, Carbon 118 (2017) 680–685.

[48] M. Kijima, D. Fujiya, T. Oda, M. Ito, Efficient thermal conversion of polyyne-type conjugated polymers to nano-structured porous carbon materials, J. Therm. Anal. Calorim. 81 (2005) 549–554.

[49] S.J. Prince, The pyrolysis of toluene, Can. J. Chem. 40 (1962) 1310–1317.

[50] V. Amendola, G. Rizzi, S. Polizzi, M. Meneghetti, Synthesis of gold nanoparticles by laser ablation in toluene: Quenching and recovery of the surface Plasmon absorption, J. Phys. Chem. B 109 (2005) 23125–23128.

[51] A. Oya, H. Marsh, Phenomena of catalytic graphitization, J. Mater. Sci. 17 (1962) 309–322.